Predicting in- and out-of-plane damage evolution in fiber-reinforced composites

W. Wilson
Fokker Landing Gear B.V., The Netherlands

Abstract*: Fokker Landing Gear has a history in development of composite technology for landing gear applications. In order to successfully design and qualify composite landing gear parts it is essential to be able to reliably predict the mechanical and failure behavior of the composite material. Therefore the goal of this study was to develop, calibrate and validate a material model which can be used to reliably predict the failure behavior of fiber-reinforced composites. In the developed material model the fibers and resin are modelled as separate materials with their own specific material and failure behavior. The interaction between the fibers and resin is accounted for using a (proprietary) modified Mori-Tanaka approach. For the resin both the plasticity and damage behavior is included. For fiber failure new damage laws have been developed. Cohesive surfaces are used to model the delamination behavior. The implementation of this material model and cohesive damage laws is done in Abaqus/Standard. Comparison with test data showed that with the material model the failure behavior in many different tests could be predicted very well.*

Keywords: Composites, Constitutive Model, Damage, Delamination, Fabrics, Failure, Landing Gear, User-Defined Material,

1. Introduction

Fokker Landing Gear has a history in the development of composite technology for aircraft landing gear applications. Due to the highly safety critical nature of landing gear components, in order to successfully design and qualify these components it is essential to be able to reliably predict the mechanical and failure behavior of the composite material.
Traditional models used for modelling composites are in most cases linear elastic and use failure criteria (in most cases only valid for uni-directional materials) to predict the moment of failure. Hence, they do not take into account the nonlinear behavior of the resin and the actual damage initiation and damage evolution. With these traditional models the mechanical behavior and failure moment of thin undisturbed composite sections can be predicted relatively well. However, for thick composites and especially around stress concentration (e.g. open holes, pin loaded holes) the traditional models under predict the failure loads by a large margin (e.g. Chang et al., 1984; Whitworth et al., 2003). Over the last years more detailed material models have been developed that include the effect of resin damage and plasticity (e.g. Johnson, 2001; Chen et al., 2014).

Although big steps forward have been made, with the models currently available it was not possible to reliably predict the failure behavior of the composite materials using textile (woven) fiber reinforcements. In order to address this issue Fokker Landing Gear has developed a new material model for modeling composites (Wilson, 2011, 2013) with the capability of modelling textiles composites. In this material model the fibers and resin are modelled as separate materials with their own specific thermo-mechanical and failure behavior. The interaction between the fibers and resin is accounted for using a (proprietary) modified Mori-Tanaka approach. The implementation of this material model and cohesive damage laws is done in Abaqus/Standard.

Previously it has been shown that composites with different textile architecture (2x2 twill fabric layers and 2D braided layers with varying angles) can be described with the same set of material data (Wilson, 2011). It was also shown that this material model is capable of predicting failure around stress concentrations (Wilson, 2013).

The goal of the current study was to further improve this model with new failure laws and to incorporate the plasticity behavior of the resin, such that it can more reliably predict the failure behavior of fiber-reinforced composites.

2. Method

2.1 Material model

2.1.1 Total stress

The total stress in the material is given by

$$\boldsymbol{\sigma}_{tot} = \left(1 - \sum_{i=1}^{totf} \rho_f^i\right)\boldsymbol{\sigma}_r + \sum_{i=1}^{totf} \rho_f^i \boldsymbol{\sigma}_f^i \,, \qquad \text{Equation 1}$$

where $\boldsymbol{\sigma}_r$ and $\boldsymbol{\sigma}_f$ are the total resin and fiber stress tensors, respectively, *totf* the number of fiber directions and ρ_f^i the fiber volume fraction in the *i*-th direction $\vec{e}_f^{\,i}$, respectively. When the strains in a composite are relatively low, it can be assumed that the relative volume fractions of the resin and fiber stay constant during deformation. Hence, ρ_f^i is taken as a constant.

2.1.2 Microstructure model

Following the rules of mixtures the total strain in the material is given by

$$\boldsymbol{\varepsilon} = \left(1 - \sum_{i=1}^{totf} \rho_f^i\right)\boldsymbol{\varepsilon}_r + \sum_{i=1}^{totf} \rho_f^i \boldsymbol{\varepsilon}_f^i \,, \text{ Equation 2}$$

where $\boldsymbol{\varepsilon}_r$ and $\boldsymbol{\varepsilon}_f^i$ are the resin and fiber strain tensors, respectively. When we express ($\boldsymbol{\varepsilon}_f^i$) as a function of the resin strain ($\boldsymbol{\varepsilon}_r$)

$$\boldsymbol{\varepsilon}_f^i = {}^4\mathbf{A}_f^i : \boldsymbol{\varepsilon}_r \,, \text{ Equation 3}$$

this Equation 2 becomes

$$\boldsymbol{\varepsilon} = \left(1 - \sum_{i=1}^{totf} \rho_f^i\right)\boldsymbol{\varepsilon}_r + \sum_{i=1}^{totf} \left(\rho_f^i \, {}^4\mathbf{A}_f^i\right) : \boldsymbol{\varepsilon}_r \,, \text{ Equation 4}$$

from which follows that

$$\boldsymbol{\varepsilon}_r = \left[\left(1 - \sum_{i=1}^{totf} \rho_f^i\right){}^4\mathbf{I} + \sum_{i=1}^{totf} \left(\rho_f^i \, {}^4\mathbf{A}_f^i\right)\right]^{-1} : \boldsymbol{\varepsilon} \,. \text{ Equation 5}$$

Here ${}^4\mathbf{A}_f^i$ is the strain concentration tensor that relates the (local) fiber strain to the resin strain, which is computed using a proprietary modified Mori-Tanaka approach (based on Mori & Tanaka, 1973).

2.1.3 Fiber properties

The fibers are assumed to behave linear elastic and anisotropic, with a different stiffness in compression and tension. Fiber damage is assumed to be a brittle fracture. Although it is assumed that a fiber fails immediately once damaged, the total damage in a fiber bundle is assumed to evolve more gradually, mainly due to the differences in fiber orientations and resin distribution around the fibers (which influences the local fiber stresses). The following function for the evolution of the damage parameter D_f is used

$$D_f = \left(\frac{\kappa_{c,f}}{\kappa_f} \right) \left(\frac{\kappa_f - \kappa_{i,f}}{\kappa_{c,f} - \kappa_{i,f}} \right). \text{ Equation 6}$$

$\kappa_{i,f}$ and $\kappa_{c,f}$ are the values of history parameter κ_f at which damage initiation starts and at which the fibers have completely failed. For tensile failure the history parameter κ_f is set equal to the maximum fiber strain over time. The function for κ used for compressive failure is proprietary to Fokker Landing gear, but is based on the assumption that fiber micro-buckling is dependent on the compressive fiber strain, effective resin stiffness and the out-of-plane strains (compressive out-of-plane strains are assumed to inhibit micro-buckling and tensile out-of-plane strains are assumed to promote micro-buckling).

2.1.4 Resin properties

The resin is assumed to have an elasto-plastic behavior, with linear elastic behavior up to the point where the material starts to plastically deform. For the plastic behavior an exponential Nadai Ludwik hardening law is chosen.

$$\sigma_y(t) = \sigma_{y,0} \left(1 + \frac{\bar{\varepsilon}_{r,p}(t)}{\varepsilon_0} \right)^n \text{ Equation 7}$$

where $\bar{\varepsilon}_{r,p}$ is the plastic equivalent strain, $\sigma_{y,0}$ the initial yield stress and ε_0 and n material parameters. Assuming von Mises plasticity the following flow rule is used

$$\dot{\boldsymbol{\varepsilon}}_{r,p} = \frac{3}{2} \frac{\bar{\varepsilon}_{r,p}}{\bar{\sigma}_r^{ip}} \boldsymbol{\sigma}_r^{dip} \text{ Equation 8}$$

with $\bar{\sigma}_r^{ip}$ the in-plane equivalent von Mises stress, and $\boldsymbol{\sigma}_r^{dip}$ the in-plane deviatoric part of the resin stress tensor. For the resin damage the following function is used (Johnson, 2001)

$$D_r = \alpha \log \left(\frac{\bar{\sigma}_r^{ip}}{F_r} \right) \text{ Equation 9}$$

where F_r is the in-plane von Mises stress at which damage initiates and α a positive constant that determines the rate of damage evolution.

2.1.5 Mesh dependency

When a material gets damaged, part of the material can no longer carry any loads. Due to this the effective stiffness of the material decreases. Analyses with such softening behavior are normally very sensitive to mesh-dependency. In Abaqus the Hillerborg's fracture energy proposal (Hillerborg et al., 1976) is available which for most cases can (partly) alleviate the mesh-dependency. A more general, but computationally less efficient, method for alleviating mesh-dependency is a nonlocal damage theory (e.g. Pijaudier-Cabot and Bazant, 1987; Bazant and Pijaudier-Cobot, 1988; Comi, 2001). In the non-local damage theory the local strain ε that determines the damage initiation is replaced by a nonlocal strain $\bar{\varepsilon}$. This nonlocal strain is taken as a weighted average of the strain within a volume *V*.

$$\bar{\varepsilon}(\vec{x}) = \frac{1}{V}\int_V g(\vec{\xi})\varepsilon(\vec{x}+\vec{\xi})dV = \frac{\sum_{i=1}^{n} V(\vec{\xi}_i)\exp\left(-\frac{\vec{\xi}_i^{\,2}}{2l^2}\right)\varepsilon_i(\vec{\xi}_i)}{\sum_{i=1}^{n} V(\vec{\xi}_i)\exp\left(-\frac{\vec{\xi}_i^{\,2}}{2l^2}\right)}, \text{ Equation 10}$$

where *l* is the length scale of the material, *V* is the volume of punt *i* with a distance $\vec{\xi}_i$ from the current location $\vec{x}$.

For modelling failure in composites, next to alleviating mesh-dependency there is another reason to use a non-local method. As mentioned in the previous paragraph compressive fiber failure is generally assumed to occur via micro-buckling of the fibers. For micro-buckling to occur, high strains or stresses should be present over a certain length of the fiber. Hence, very local stress or strain peaks will probably not lead to micro-buckling. As the nonlocal method uses an average strain over a certain area, it will filter out these very local strain peaks. For the tensile failure of fiber the Hillerborg's fracture energy proposal is used.

2.2 Delaminations

2.2.1 Initiation laws

Mode 1 delaminations are assumed to occur due to excessive tensile out-of-plane stresses alone.

$$\frac{\sigma_{33}}{F_{33}} \geq 1, \text{ Equation 11}$$

The initiation and growth of mode 2 delaminations in composites is mainly governed by the transverse shear stresses (τ_{13}, τ_{23}). Compressive out-of-plane stresses are known to inhibit the initiation and growth of mode 2 delaminations while tensile out-of-plane stresses are known to promote the initiation and growth of mode 2 delaminations (Lecuyer and Engrand, 1992). A law for damage initiation based on the above assumptions is given by

$$\frac{\max(\tau_{13},\tau_{2,3})}{F_{tvsh}} + \beta\sigma_{33} \geq 1, \text{ Equation 12}$$

where F_{tvsh} is the transverse shear strength and β a positive constant. Mode 3 failure is assumed to occur by the same rules as Mode 2.

2.2.2 Implementation

To implement Equation 11 and 12 in Abaqus/Standard the maximum stress criterion is used.

$$\left|\frac{\tau_{13}}{F_{13}}\right|, \left|\frac{\tau_{23}}{F_{23}}\right|, \left|\frac{\sigma_{33}}{F_{33}}\right| \geq 1, \text{ Equation 13}$$

To implement Equation 12 into Equation 13 F_{13} and F_{23} have to be made dependent on the out-of-plane stress (σ_{33}). To do this Equation 13 has to be rewritten to

$$\frac{\max\left(|\tau_{13}|,|\tau_{23}|\right)}{F_{tvsh} - \beta^{*}\sigma_{33}}, \left|\frac{\sigma_{33}}{F_{33}}\right| \geq 1, \text{ Equation 14}$$

where β^{*} is given by β/F_{tvsh}. The implementation of this damage initiation law in Abaqus/Standard is described in detail in reference (Wilson, 2013).

2.3 Implementation in Abaqus and general model description

The material model as discussed in the section 2.1 (including the nonlocal damage theory) has been implemented in Abaqus/Standard using the user-subroutines UMAT and USDFLD. For more details about the implementation see (Wilson, 2013). The element deletion option is used to delete elements in which the fibers have completely failed (this option is available in combination with UMAT since Abaqus v6.14-1). All finite element models used in this paper consisted of C3D8R elements with enhanced hourglass control. When possible due to symmetry, only half of the total test sample was modeled. Each ply was modeled as a separate element layer. The layers were tied together using cohesive surfaces. Initiation and growth of delaminations was included in the material description of the cohesive surfaces (see paragraph 2.2). Surface-to-surface small-sliding contact was used for the cohesive surfaces. Contact between samples and the test fixtures was modelled using surface-to-surface finite sliding contact. Boundary conditions were chosen such that they mimic the test conditions most accurately.

2.4 Determination of unknown material parameters

For the current study a composite material consisting of a combination of a quasi-UD 2x2 twill fabric and braids of carbon fibers embedded in an epoxy resin was used. As the actual material data is proprietary to Fokker Landing Gear only relative differences between test and numerical data will be given. Calibration of the unknown material properties is done in the following sequence:

1. Linear stiffness properties (Young's moduli and Poisson's ratios of the fiber and resin and 2 shape parameters) (number of parameters = 7)

2. Non-linear resin properties (Plastic and damage behavior of resin) (number of parameters = 7)
3. Delamination properties (Mode 1 and 2 failure) (number of parameters = 3)
4. Tensile failure properties of the fibers (number of parameters = 2)
5. Compressive failure properties of the fibers (number of parameters = 3)

For step 1 to 4 only samples consisting of the 2x2 twill fabric were used. For Step 5 a combination of the 2x2 twill fabric and braids was used. In the next paragraphs the used calibration methods are briefly described.

2.4.1 Linear resin and fiber properties

Isight 5.9 was used to calibrate the linear material properties (Young's moduli and Poisson's ratios of the fiber and resin). As optimization method the "pointer method" is used. The simflow that was used is depicted in Figure 1. To make the simflow as efficient as possible several coupon tests were modeled within one Abaqus simulation. Furthermore, three Abaqus/Standard simulations were run in parallel in the Isight simflow (Figure 1A). In total 7 coupon test were simulated:

- Compression in 0º and 90 º direction (ASTM D695)
- Tension in 0º and 90 º direction (ASTM D3039)
- In-plane shear test (ASTM D3518)
- 2 different 3 point bending tests (ASTM D2344)

Displacements and reaction forces were extracted from the Abaqus simulations using History output. Using the Calculator component ("Compute stiffnesses" component in Figure 1A) the sample stiffnesses were computed from the history data, after which the Excel component was used to read in the stiffnesses as computed from test data. The Calculator component was then used to compute the relative errors between the test data. As objective function the sum of all relative errors is used.

2.4.2 Non-linear resin properties

Isight 5.9 was used to calibrate the nonlinear material resin properties (Plastic and damage behavior of the resin). As optimization method the "pointer method" is used. To be able to make a distinction between the plasticity and damage behavior an in plane shear test with cyclic loading was used (Paepegem et al., 2006). The Isight simflow (Figure 1B) consisted of an Abaqus component in which the in-plane shear test is simulated and a Matlab component in which the stiffness, plasticity and damage as function of the shear strain are determined and compared to the test data. As an objective function the sum of the relative errors of these curves is used.

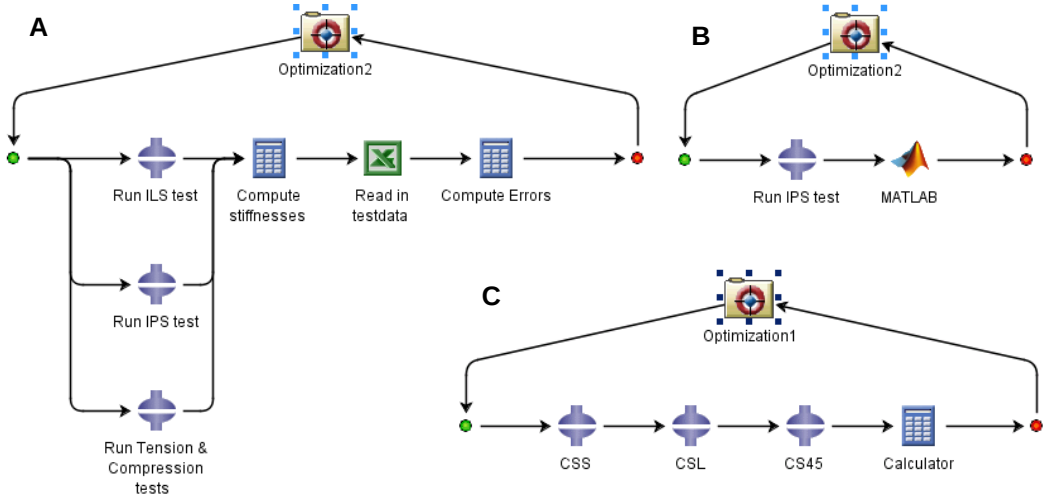

Figure 1. Isight simflow for the optimization of A) linear stiffness properties, B) non-linear resin properties, and C) compressive fiber failure properties.

2.4.3 Delamination properties

To determine the delamination properties first the mode 1 properties were determined using a peel test (ASTM D5528). The two unknown material properties are the damage initiation stress and the energy release rate parameter (G_{1c}). The latter can be directly determined from test data. The damage initiation stress was obtained by manual optimization.

For the optimization of the Mode 2 parameters 3 different 3-point bending tests (ILS1 $[0^f/90^f]_{3s}$, ILS2 $[90^f/0^f]_{3s}$, ILS3 $[0^f_6]$[1]) were used (ASTM D2344). The unknown parameters for the Mode 2 failure were determined by a manual optimization. To minimize the number of unknown material parameters, the following relation between the τ_{13} and τ_{33} was used (Turon et al., 2010).

$$\tau_{13} = \tau_{33}\sqrt{\frac{G_{IIc}}{G_{Ic}}} \text{ , Equation 15}$$

2.4.4 Tensile failure of fibers

For the determination of the tensile fiber failure properties 2 tensile tests were used (ASTM D3039), one in warp (0º) and one in weft (90º) direction. Tensile failure strains ($\kappa_{i,f}$ from Equation 7) were directly taken from the test data. The damage evolution parameters ($\kappa_{c,f}$ from Equation 7) were determined by manual optimization.

2.4.5 Compressive failure of fibers

For the determination of the compressive 0º-fiber failure properties 3 compression tests (COMP1 $[45^f/-45^f/0^f_4]_s$, COMP2 $[45^f/-45^f/0^f_3/45^f/-45^f/0^f_3/-45^f/45^f]$ and COMP3 $[0^{\pm b45}_3,0^f_4]_s$)[1] were used. The

[1] Here *f* means that the ply consist of the 2x2 twill fabric, and ±b45 mean the ply consists of a ±45º braid.

90º -fiber failure properties were manually derived from the 0º-fiber failure properties. The calibration (optimization) was done using Isight 5.9 (Figure 1C). As optimization method the "pointer method" is used. As an objective function the sum of the relative errors in failure load was used.

2.5 Validation

For validation of the model the following tests were used.

Tensile test

The tensile test was performed according to ASTM D3039 with a tapered specimen with a layup of $[0^{\pm 45b}/0_4^f]_s$ (Figure 2). The FEA model consisted 3324 C3D8R elements with enhanced hourglass control. Due to symmetry, in the FEA models only a half of the total sample was modeled.

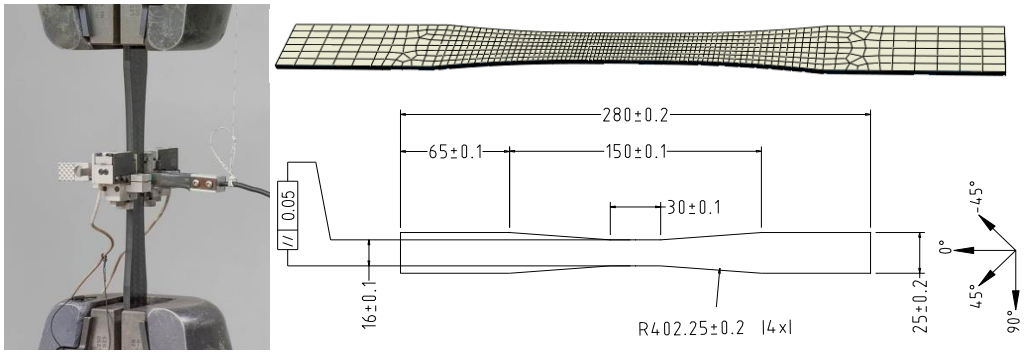

Figure 2. Top-Left) Photograph of tensile test setup; Top-Right) Dimensions; Bottom) FEA mesh.

Compression test

The compression test was performed according to ASTM D3410-03 with a modified sample (layup of $[0^{\pm 45b}/0_4^f]_s$) and a NASA short block compression fixture (Figure 3). The FEA model consisted 4534 C3D8R elements with enhanced hourglass control. Due to symmetry, in the FEA models only a half of the total sample was modeled.

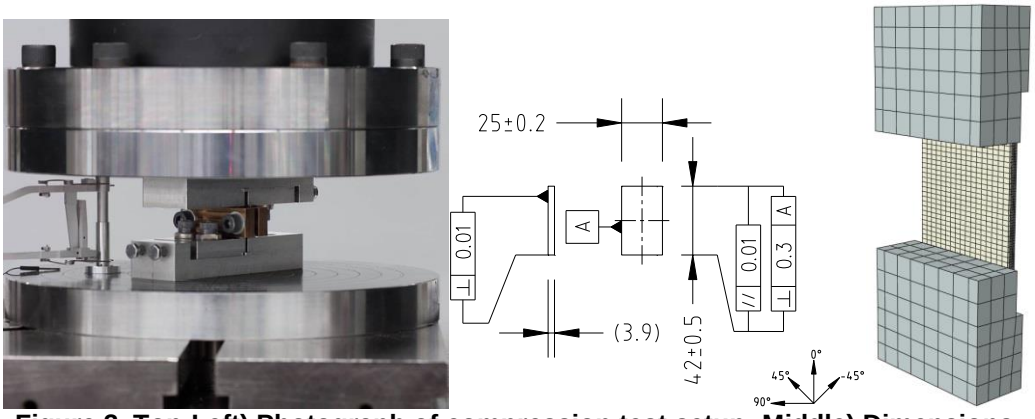

Figure 3. Top-Left) Photograph of compression test setup; Middle) Dimensions; Right) FEA mesh.

Bearing compression & tension

The bearing tests (compression & tension) were performed according to ASTM D5961-09 (Figure 4). The tested samples had a layup of $[0^{\pm 45b}/0_4^f/+45^f/-45^f]_s$. The loading pin had a diameter of 19.03 mm. The FEA models consisted of 6508 and 8131 C3D8R elements with enhanced hourglass control, for the compression and tension test respectively. The pins were modelled as an analytical rigid. The parts inside the lower clamps was not included in the models, instead the bottom planes were fixed in all directions. Due to symmetry, in the FEA models only half of the total sample was modeled.

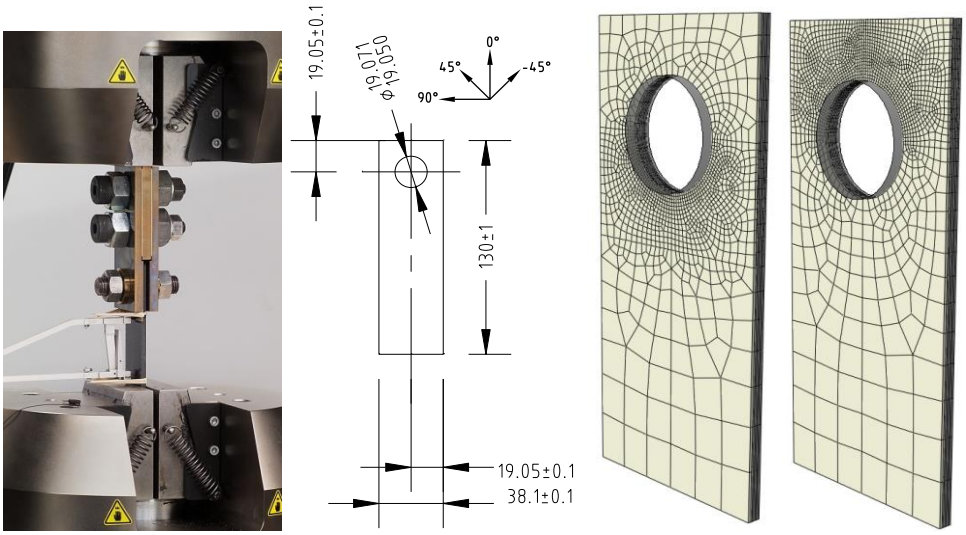

Figure 4. Left) Photograph of bearing compression test setup; Middle) Dimensions; Right) FEA mesh (left: compression; right: tension).

Open hole compression

The open hole compression tests were performed according to ASTM D6484 (Figure 5). The tested samples had a layup of $[0^{\pm 45b}/0_4^f/0^{\pm 45b}/0^{\pm 45b}/0^{\pm 45b}/0_4^f/0^{\pm 45b}]$. The FEA model consisted of 7712 C3D8R elements with enhanced hourglass control. Due to symmetry, in the FEA models only half of the total sample was modeled.

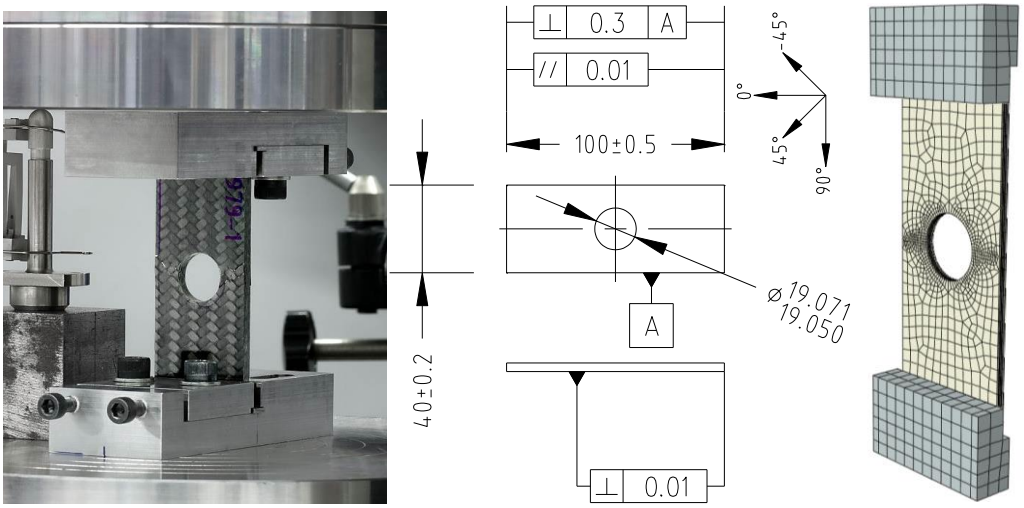

Figure 5. Left) Photograph of open hole compression test setup; Middle) Dimensions; Right) FEA mesh.

3. Results

3.1 Calibration of material properties

3.1.1 Linear resin and fiber properties

The resulting errors between the FEA predictions and test data are given in Table 1.

Table 1: Resulting error [%] between FEA model and mean test data

E_{CE0}	E_{CE90}	E_{TE0}	E_{TE90}	υ_{TE0}	E_{ips}	υ_{ips}	E_{ILS1}	E_{ILS2}
0	0	2	0	1	3	4	3	1

3.1.2 Non-linear resin properties

In Figure 6 the shear stress, resin damage and plastic shear strain are plotted as a function of the axial or shear strain for both the average test data and FEA data. The FEA results corresponded very well with the test data.

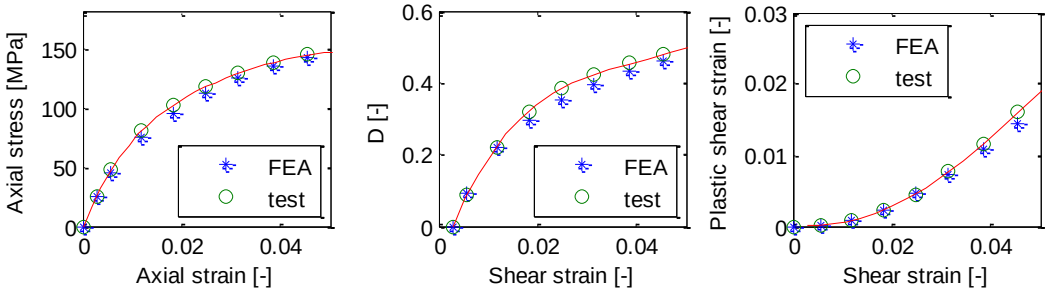

Figure 6. Resulting nonlinear resin response as a function of the shear strain. Left) Shear stress, Right) Resin damage, Bottom) Plastic shear strain.

3.1.3 Delamination properties

In Figure 7 the resulting force-displacement graph of the FEA model and test data is given for the G1c peel test and one 3-point bending test (ILS3). For the other 2 3-point bending tests the relative difference between the FEA and test data was approximately 5%.

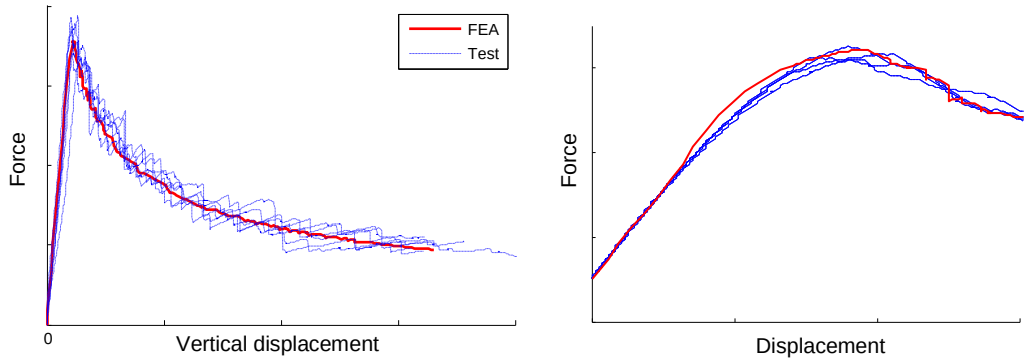

Figure 7. Left) Force-displacement graph of peel test, Right) Force displacement graphs of 3 point bending test ILS3 (blue=no damage; red=failed).

3.1.4 Tensile failure of fibers

The resulting error between the FEA predictions and test data for both the 0º and 90º failure was <1%. The failure modes of both simulations corresponded very well to the test data.

3.1.5 Compressive failure of fibers

The computed failure loads corresponded very well with the test results (see Table 2).

Table 2: Resulting Errors in compression strength

	COMP1	COMP2	COMP3
ERROR [%]	+3	-3	+5

3.2 Validation

For the validation tests the relative errors between the predicted failure loads and the test data are given in table 3.

Table 3: Errors between FEA and testdata

	Error [%]				
	Full model	No fiber compression failure	No fiber tension failure	No resin plasticity & damage	No delaminations
Tension	+1				
Compression	+6				
Open hole compression	-2	>100	-2	+6	-3
Bearing tension	-7	+2	-6	+36	+1
Bearing compression	+1	+94	+1	+69	+5

In figure 8 to 10 photographs of the failed open hole compression and bearing tests samples are given together with the deformed meshes of the failed FEA simulations. The predicted failure modes corresponded very well with failure modes seen in the tests. For all tests a combination of resin damage/plasticity, delaminations and fiber damage was seen. To study the effect of these different failure mechanisms on the final failure of the samples additional simulations were performed in which each failure mechanism was selectively turned off. The results are given in Table 3. The open hole compression test seemed to be mainly dependent on the compressive failure. Although the resin plasticity and damage also slightly influenced the results (considering that the compressive failure is dependent on resin plasticity and damage). For the bearing tension and compression test the influence of the resin damage and plasticity was much larger. In the bearing tension test both compressive and tensile fibers failure occurred almost simultaneously, which can be the reason that failure can be relatively well be predicted by including just only one of these failure mechanism. All tests were slightly dependent on the inclusion of delamination initiation and growth.

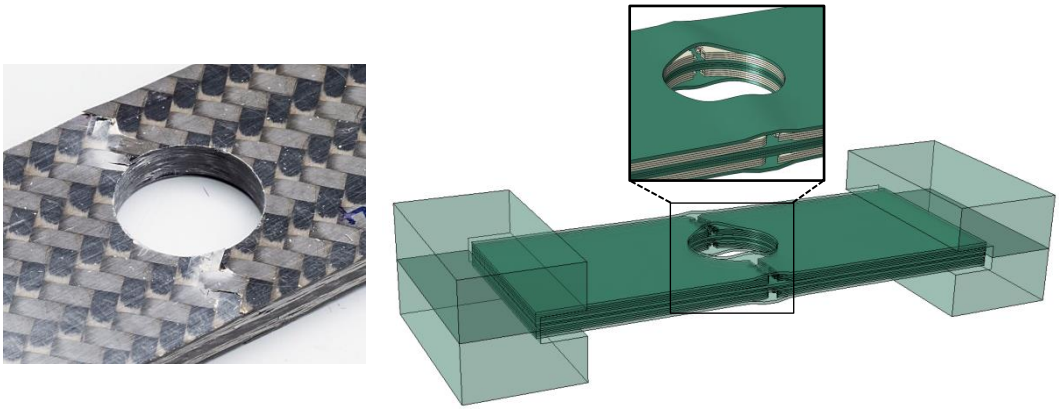

Figure 8. Left) photograph of failed open hole compression test specimen, Right) Deformed FEA model after failure

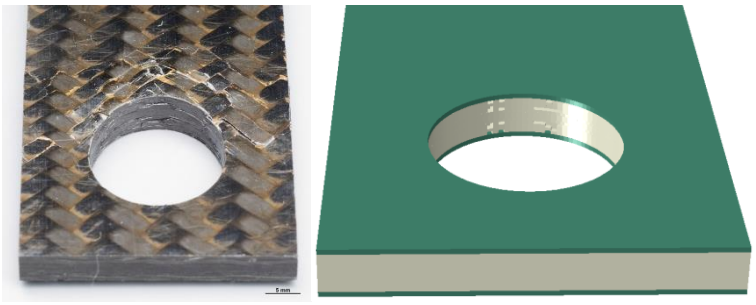

Figure 9. Left) photograph of failed bearing compression test specimen, Right) Deformed FEA model after failure

Figure 10. Left) photograph of failed bearing tension test specimen, Right) Deformed FEA model after failure

4. Discussion

In order to successfully design and qualify safety critical composite parts, it is essential to be able to reliable predict the mechanical and failure behavior of composite materials in "disturbed" areas. Therefore the goal of this study was to develop, calibrate and validate a material model which can be used to reliably predict the failure behavior of fiber-reinforced composites.
For the current study, the model of Wilson (2013) was extended to include the plasticity of the resin, updated failure laws and an improved microstructure model. In this material model the fibers and resin are modelled as separate materials with their own specific material and failure behavior. The interaction between the fibers and resin is accounted for using a (proprietary) modified Mori-Tanaka approach. For the resin both the plasticity and damage behavior is included. For fiber failure new damage laws have been developed. Cohesive surfaces are used to model the delamination behavior. The implementation of this material model and cohesive damage laws is done in Abaqus/Standard.
The nonlinear stiffness behaviour of the model was previously validated (Wilson et al. 2011) by predicting the mechanical behaviour of braids (with different configuration) using material properties that were fitted on the 2x2 twill fabric data used in this paper. In the current study it is shown that also the in- and out of plane failure behaviour can be predicted very well for a large variety of loading conditions and many different layups.
During testing a failure often occurs very rapidly. After the failure it is very difficult to see how that failure was initiated and what the sequence of (possible) different failure mechanisms was. In the current study we have shown that a model as developed in the current study can be used to

explain the sequence (and importance) of the different failure mechanisms in the total failure process.
In the current study the material model was calibrated using coupon test data, and validated using element test data (including stress concentration). For a full validation the model should be validated for both additional element test and full thickness components or subcomponent.

5. References

1. Abaqus Users Manual, Version 6.14-1, Dassault Systems Simulia Corp. Providence, RI
2. Bazant, Z.P., Pijaudier-Cobot, T.G.P., Nonlocal continuum damage, localization instability and convergence, J. Appl. Mech., Vol. 55, pp.287–293, 1988
3. Chang, F. et al., Failure of Composite Laminates Containing Pin Loaded Holes, Journal of Composite Materials. vol. 18, 255-278, 1984
4. Jing-Fen Chen, Evgeny V. Morozov, Krishnakumar Shankar, Simulating progressive failure of composite laminates including in-ply and delamination damage effects, Composites Part A,, Volume 61,185-200 (2014)
5. Comi, C., A non-local model with tension and compression damage mechanisms, Eur. J. Mech. A/Solids, Vol. 20, pp.1–22. 2001
6. Hillerborg, A., M. Modeer, and P. E. Petersson, Analysis of Crack Formation and Crack Growth in Concrete by Means of Fracture Mechanics and Finite Elements, Cement and Concrete Research, vol. 6, pp. 773–782, 1976.
7. A.F. Johnson, Modelling fabric reinforced composites under impact loads, Composites Part A, Volume 32, Issue 9, Pages 1197–1206 (2001)
8. Lecuyer, F., Engrand, D., A methodology for the identification of a criterion for delamination initiation, JNC8:751-762, 1992
9. W. Van Paepegem, I. De Baere, J. Degrieck., I. Modelling the nonlinear shear stress-strain response of glass fibre-reinforced composites. part I: Experimental results. Composites Science and Technology, 66(10):1455-1464, 2006.
10. Pijaudier-Cabot, T.G.P., Bazant, Z.P. Nonlocal damage theory, J. Engng. Mech. (ASCE), Vol. 113, pp.1512–1533, 1987
11. Mori, T., Tanaka, K., 1973. Average stress in matrix and average elastic energy of materials with misfitting inclusions. Acta Metall. 21, 571–574.
12. A Turon, PP Camanho, J Costa, J Renart, Accurate simulation of delamination growth under mixed-mode loading using cohesive elements: definition of interlaminar strengths and elastic stiffness, Composite Structures 92 (8), 1857-1864, 2010
13. Whitworth, H. A., et al., Failure analysis of composite pin loaded joints., Composite Structures, vol. 59, 261–266, 2003
14. Wilson.,W., Virtual testing of composites using Abaqus., 2011 SIMULIA Customer Conference, Conference Proceedings, May 2011
15. Wilson W, Prediction of damage evolution in composites, 2013 SIMULIA Customer Conference, Conference Proceedings, May 2013